E17-2010-62

A. A. Vladimirov, D. Ihle*, N. M. Plakida

DYNAMIC SPIN SUSCEPTIBILITY OF SUPERCONDUCTING CUPRATES: A MICROSCOPIC THEORY OF THE MAGNETIC RESONANCE MODE

Submitted to «Physical Review B»

*Institut für Theoretische Physik, Universität Leipzig, D-04109, Leipzig, Germany

Владимиров А. А., Иле Д., Плакида Н. М. E17-2010-62

Динамическая спиновая восприимчивость купратных сверхпроводников:
микроскопическая теория магнитной резонансной моды

Сформулирована микроскопическая теория динамической спиновой восприимчивости в сверхпроводящей фазе в рамках $t-J$-модели. С помощью проекционной техники типа Мори для функции релаксации в терминах операторов Хаббарда получено точное представление для восприимчивости. Статическая спиновая восприимчивость вычисляется в обобщенном приближении среднего поля с учетом правила сумм. Массовый оператор вычисляется в приближении взаимодействующих мод. Спектр спиновых возбуждений рассматривается в области низкого и оптимального легирования. Обнаружено появление резонансной моды на антиферромагнитном волновом векторе $\mathbf{Q} = \pi(1,1)$ при низких температурах, вызванное сильным подавлением затухания спиновых возбуждений. Это объясняется участием спиновых возбуждений в процессе распада, в отличие от приближения случайных фаз, в котором учитывается только распад на пару частица–дырка. Щель в спектре спиновых возбуждений играет главную роль в ограничении распада по сравнению со сверхпроводящей щелью, что приводит к возникновению резонансной моды выше T_c в области низкого легирования. Получено достаточно хорошее согласие с экспериментами по неупругому рассеянию нейтронов на кристаллах YBCO.

Работа выполнена в Лаборатории теоретической физики им. Н. Н. Боголюбова ОИЯИ.

Препринт Объединенного института ядерных исследований. Дубна, 2010

Vladimirov A. A., Ihle D., Plakida N. M. E17-2010-62

Dynamic Spin Susceptibility of Superconducting Cuprates:
A Microscopic Theory of the Magnetic Resonance Mode

A microscopic theory of the dynamic spin susceptibility (DSS) in the superconducting state within the $t-J$ model is presented. It is based on an exact representation for the DSS obtained by applying the Mori-type projection technique for the relaxation function in terms of Hubbard operators. The static spin susceptibility is evaluated by a sum-rule-conserving generalized mean-field approximation, while the self-energy is calculated in the mode-coupling approximation. The spectrum of spin excitations is studied in the underdoped and optimally doped regions. The DSS reveals a resonance mode (RM) at the antiferromagnetic wave vector $\mathbf{Q} = \pi(1,1)$ at low temperatures due to a strong suppression of the damping of spin excitations. This is explained by an involvement of spin excitations in the decay process besides the particle–hole continuum usually considered in random-phase-type approximations. The spin gap in the spin-excitation spectrum at $\mathbf{Q}$ plays a dominant role in limiting the decay in comparison with the superconducting gap which results in the observation of the RM even above T_c in the underdoped region. A good agreement with inelastic neutron-scattering experiments on the RM in YBCO compounds is found.

The investigation has been performed at the Bogoliubov Laboratory of Theoretical Physics, JINR.

Preprint of the Joint Institute for Nuclear Research. Dubna, 2010

1. INTRODUCTION

In the superconducting state the spin-excitation spectrum of high-T_c cuprates is dominated by a sharp magnetic peak at the planar antiferromagnetic (AF) wave vector $\mathbf{Q} = \pi(1,1)$ which is called *the resonance mode* (RM). It was observed that the spectral weight of low-energy spin excitations, suppressed below T_c, transfers to higher energy resulting in the RM. This was discovered at first in the optimally doped $YBa_2Cu_3O_y$ ($YBCO_y$) crystal at the energy $E_r \approx 41$ meV but later on, the RM was found in other cuprates as well (for reviews see [1–3]). In particular, the RM was observed in the single-layer $Tl_2Ba_2CuO_{6+x}$ cuprate superconductor [4] and in the electron-doped $Pr_{0.88}LaCe_{0.12}CuO_{4-\delta}$ superconductor [5]. This demonstrates that the RM is a generic feature of the cuprate superconductors and can be related to spin excitations in a single CuO_2 layer. Since the energy of the RM scales with the superconducting temperature, $E_r \approx 5.3 k_B T_c$ [2], it has been argued that it might constitute the bosonic excitation mediating superconducting pairing in cuprates which has motivated an extensive study of the RM phenomenon (see, e.g., [3]).

The spin-excitation dispersion close to the RM exhibits a peculiar «hourglass»-like shape with upward and downward dispersions. Whereas the RM energy changes with doping, no essential temperature dependence of it was found. In the optimal doping region the RM and both dispersion branches vanish above T_c. In the strongly underdoped YBCO crystal only the downward dispersion vanishes above T_c, whereas the upward dispersion and the RM are observed in the normal pseudogap state. In particular, a well-defined resonance peak at $E_r \approx 33$ meV was found in the $YBCO_{6.5}$ crystal in the oxygen ordered ortho-II phase with $T_c = 59$ K at hole doping $p = 0.09$ [6, 7]. At low temperature, $T \sim 8$ K, the RM revealed a much higher intensity than in optimally doped crystals, and it was also seen with less intensity even at $T \simeq 1.4\,T_c$. The RM was not found in the highly underdoped $YBCO_{6.35}$ crystal with $T_c = 18$ K at $p = 0.06$ [8]. Instead, a two-scale dynamics at low temperatures was observed: a broad spectrum of relaxation-type excitations at $\mathbf{Q}$ and a slowly fluctuating narrow central mode characteristic for a short-range spin-glass structure. It may be suggested that a disordered quasi-static short-range spin-glass structure destroys the sharp dynamic RM.

To explain the RM in superconducting cuprates, a number of theoretical models was proposed. Two basic approaches in the theory of the RM can be singled out. In the first one, the RM is considered as a particle–hole bound state, usually referred to as a spin-1 exciton (for a review see [3]). The state is formed below the continuum of particle–hole excitations which is gapped at a threshold energy $\omega_c \leqslant 2\Delta(\mathbf{q}^*)$ determined by the superconducting d-wave gap $2\Delta(\mathbf{q}^*)$ at a particular wave vector $\mathbf{q}^*$ on the Fermi surface (FS). In this approach a model of itinerant electrons is assumed, and the dynamic spin susceptibility (DSS) is calculated within the random phase approximation (RPA) in the weak correlation limit of the Hubbard model, $U \ll t$ (see, e.g., [9, 10] and references therein). Both the downward and upward dispersions were found. To describe the underdoped regime close to the insulating (and AF) state, where a model of itinerant electrons cannot be justified, a phenomenological spin-fermion model was used (see, e.g., [3]).

In favor of the spin-exciton scenario, the neutron scattering studies of the RM in the slightly overdoped $Bi_2Sr_2CaCu_2O_{8+\delta}$ (Bi-2212) crystal [11] and in $Y_{1-x}Ca_xB_2Cu_3O_{6+x}$ (Y-CaBCO) compounds [12] are discussed. In particular, the global momentum shape of the measured magnetic excitations is quantitatively described within the spin-exciton model with parameters inferred from angle-resolved photoemission experiments on Bi-2212 or electronic Raman scattering experiments on Y-CaBCO. However, the temperature dependence of the RM energy was not studied which should be observed in the spin-exciton model due to the temperature dependence of the superconducting gap.

In the second approach, the importance of strong electron correlations is stressed which are usually treated within the t–J model suitable for consideration of low-energy spin dynamics. To take into account the projected character of the electron operators, the Hubbard operator technique [13] should be used. To deal with the Hubbard operator kinematics, a complicated diagram technique was developed [14]. In particular, a generalized RPA was elaborated to calculate the DSS by summing up bubble-type diagrams as in the original RPA. Calculations of the DSS within the Hubbard operator technique in the RPA [15] revealed a strong suppression of the spin-excitation damping below T_c due to the opening of the superconducting gap in the particle–hole continuum. This results in a sharp RM at $\mathbf{Q}$ similar to the weak-correlation limit.

To calculate the DSS within the $t-J$ model, the Mori projection technique in the equation of motion method for the relaxation function [16] has been used by several groups (see, e.g., [17–22]). This technique affords to consider the magnetic excitations of localized spins in the undoped case within the AF Heisenberg model and a crossover to the itinerant electron spin excitations in the overdoped region. In [23] and [24] we have formulated a rigorous theory of the DSS in the normal state within the Mori-type projection technique for the relaxation function in terms of Hubbard operators. The obtained results, both for the static properties

(like the staggered magnetization at $T = 0$, the uniform static susceptibility, and the AF correlation length) and for the DSS (e.g., the (ω/T)-scaling behavior of the local DSS) have shown a good agreement with available cluster calculations and neutron-scattering data.

To clarify some of the open problems in describing the RM phenomenon (e.g., the appearance of the RM above $T_{\rm c}$), in the present paper we extend our microscopic theory [23] and [24] to the superconducting state. Although our general formulation for the DSS is similar to the original Mori memory function approach used in [17], in the previous studies of the t–J model only the bubble-type diagrams similar to the RPA were considered which ignores the important role of spin excitations in the decay process. The energy gap at the AF wave vector $\mathbf{Q}$ of the order of the RM energy $E_{\rm r}$ in the spin-excitation spectrum strongly reduces the damping at low temperatures, $T \ll E_{\rm r} \simeq 5\, k_{\rm B}T_{\rm c}$, which results in the emergence of a sharp peak in the spectral function, the RM excitation. In the low doping region, where the damping is extremely small, the RM is found even above $T_{\rm c}$. In the overdoped region, at hole concentration $\delta \sim 0.2$ and high $T_{\rm c}$, the spin-excitation damping becomes large and the opening of the superconducting gap enhances the intensity of the RM, so that it becomes observable only below $T_{\rm c}$. So, as compared the spin-exciton scenario, we propose an alternative explanation of the RM that is driven by the spin gap instead of the superconducting gap $2\Delta_0$. A good agreement of our results for the temperature and doping dependence of the spin-excitation spectrum and the RM with inelastic neutron-scattering experiments provides a strong support for the proposed theory.

In the next section we present the basic formulas for the DSS and the self-energy which are a generalization of our theory in [24] to the superconducting state. Numerical results for the spin-excitation spectra are given in Sec. 3, where the temperature and doping dependence of the damping and the RM are discussed. The conclusion is given in Sec. 4. Details of the calculations within the mode coupling approximation (MCA) are presented in Appendix.

2. RELAXATION-FUNCTION THEORY

2.1. Dynamic Spin Susceptibility. It is convenient to consider the $t-J$ model in the Hubbard operator representation

$$H = -\sum_{i\neq j,\sigma} t_{ij} X_i^{\sigma 0} X_j^{0\sigma} - \mu \sum_{i\sigma} X_i^{\sigma\sigma} + \frac{1}{4} \sum_{i\neq j,\sigma} J_{ij} \left(X_i^{\sigma\bar{\sigma}} X_j^{\bar{\sigma}\sigma} - X_i^{\sigma\sigma} X_j^{\bar{\sigma}\bar{\sigma}} \right), \quad (1)$$

where t_{ij} is the hopping integral and J_{ij} is the exchange interaction. The Hubbard operators $X_i^{\alpha\beta} = |i,\alpha\rangle\langle i,\beta|$ describe transitions between three possible states at a site i on a square lattice: an empty state $|i,\alpha\rangle = |i,0\rangle$ and a singly occupied

state $|i,\alpha\rangle = |i,\sigma\rangle$ with spin $\sigma = \pm(1/2)$, $(\bar{\sigma} = -\sigma)$. The number and spin operators in terms of the Hubbard operators read:

$$N_i = \sum_\sigma X_i^{\sigma\sigma}, \quad S_i^\sigma = X_i^{\sigma\bar{\sigma}}, \quad S_i^z = \sum_\sigma \sigma X_i^{\sigma\sigma}. \tag{2}$$

The Hubbard operators obey the completeness relation $X_i^{00} + \sum_\sigma X_i^{\sigma\sigma} = 1$ which preserves rigorously, contrary to the slave-boson approach, the constraint of no double-occupancy of any lattice site. The Hubbard operators have the commutation relations $\left[X_i^{\alpha\beta}, X_j^{\gamma\delta}\right]_\pm = \delta_{ij}\left(\delta_{\beta\gamma}X_i^{\alpha\delta} \pm \delta_{\delta\alpha}X_i^{\gamma\beta}\right)$ which results in the *kinematic interaction*. Here, the upper sign pertains to Fermi-type operators like $X_i^{0\sigma}$ changing the number of electrons, and the lower sign pertains to Bose-type operators, such as the number operator or the spin operators, Eq. (2). The chemical potential μ is determined from the equation for the average electron density $n = \langle N_i\rangle = 1 - \delta$, where $\delta = \langle X_i^{00}\rangle$ is the hole concentration.

In [23], applying the Mori-type projection technique [16], elaborated for the relaxation function, we have derived an exact representation for the DSS $\chi(\mathbf{q},\omega)$ related to the retarded commutator Green function (GF) (see [25]),

$$\chi(\mathbf{q},\omega) = -\langle\langle S_\mathbf{q}^+ | S_{-\mathbf{q}}^-\rangle\rangle_\omega = \frac{m(\mathbf{q})}{\omega_\mathbf{q}^2 + \omega\Sigma(\mathbf{q},\omega) - \omega^2}, \tag{3}$$

where $m(\mathbf{q}) = \langle[i\dot{S}_\mathbf{q}^+, S_{-\mathbf{q}}^-]\rangle = \langle[\,[S_\mathbf{q}^+, H],\, S_{-\mathbf{q}}^-]\rangle$, and $\omega_\mathbf{q}$ is the spin-excitation spectrum in a generalized mean-field approximation (GMFA). The self-energy is given by the many-particle Kubo–Mori relaxation function

$$\Sigma(\mathbf{q},\omega) = [1/m(\mathbf{q})]((-\ddot{S}_\mathbf{q}^+| - \ddot{S}_{-\mathbf{q}}^-))_\omega^{(\mathrm{proper})}, \tag{4}$$

where $-\ddot{S}_\mathbf{q}^\pm = [\,[S_\mathbf{q}^\pm, H], H]$ (for details see [23]). The Kubo–Mori relaxation function and the scalar product are defined as (see, e.g., [26])

$$((A|B))_\omega = -i\int_0^\infty dt e^{i\omega t}(A(t), B) \tag{5}$$

and

$$(A(t), B) = \int_0^\beta d\lambda\langle A(t - i\lambda)B\rangle, \quad \beta = 1/k_\mathrm{B}T, \tag{6}$$

respectively. The «proper» part of the relaxation function (4) does not contain parts connected by a zero-order single relaxation function which corresponds to the projected time evolution in the original Mori projection technique [16]. The spin-excitation spectrum is given by the spectral function defined by the imaginary part of the DSS (3),

$$\chi''(\mathbf{q},\omega) = \frac{-\omega\,\Sigma''(\mathbf{q},\omega)\; m(\mathbf{q})}{[\omega^2 - \omega_\mathbf{q}^2 - \omega\Sigma'(\mathbf{q},\omega)]^2 + [\omega\,\Sigma''(\mathbf{q},\omega)]^2}, \tag{7}$$

where $\Sigma(\mathbf{q},\omega+i0^+)=\Sigma'(\mathbf{q},\omega)+i\Sigma''(\mathbf{q},\omega)$ and $\Sigma'(\mathbf{q},\omega)=-\Sigma'(\mathbf{q},-\omega)$ and $\Sigma''(\mathbf{q},\omega)=\Sigma''(\mathbf{q},-\omega)<0$ are the real and imaginary parts of the self-energy, respectively.

2.2. Static Susceptibility. The general representation of the DSS (3) determines the static susceptibility $\chi_{\mathbf{q}}=\chi(\mathbf{q},0)$ by the equation

$$\chi_{\mathbf{q}}=(S^+_{\mathbf{q}},S^-_{-\mathbf{q}})=m(\mathbf{q})/\omega^2_{\mathbf{q}}. \tag{8}$$

To calculate the spin-excitation spectrum $\omega_{\mathbf{q}}$ the equality

$$m(\mathbf{q})=(-\ddot{S}^+_{\mathbf{q}},S^-_{-\mathbf{q}})=\omega^2_{\mathbf{q}}\,(S^+_{\mathbf{q}},S^-_{-\mathbf{q}}) \tag{9}$$

is used, where the correlation function $(-\ddot{S}^+_{\mathbf{q}},S^-_{-\mathbf{q}})$ is evaluated in the GMFA by a decoupling procedure in the site representation as described in [24]. This procedure is equivalent to the MCA for the equal-time correlation functions. This results in the spin-excitation spectrum

$$\begin{aligned}\omega^2_{\mathbf{q}}=8t^2\lambda_1(1-\gamma_{\mathbf{q}})(1-n-F_{2,0}-2F_{1,1})+\\ +4J^2(1-\gamma_{\mathbf{q}})\big[\lambda_2\frac{n}{2}-\alpha_1C_{1,0}(4\gamma_{\mathbf{q}}+1)+\alpha_2(2C_{1,1}+C_{2,0})\big],\end{aligned} \tag{10}$$

where t and J are the hopping integral and the exchange interaction for the nearest neighbors, respectively, and $\gamma_{\mathbf{q}}=(1/2)\,(\cos q_x+\cos q_y)$ (we take the lattice spacing a to be unity). The static electron and spin correlation functions are defined as

$$F_{n,m}\equiv F_{\mathbf{R}}=\langle X^{\sigma 0}_{\mathbf{0}}\,X^{0\sigma}_{\mathbf{R}}\rangle=\frac{1}{N}\sum_{\mathbf{q}}F_{\mathbf{q}}\mathrm{e}^{i\mathbf{qR}}, \tag{11}$$

$$C_{n,m}\equiv C_{\mathbf{R}}=\langle S^-_{\mathbf{0}}\,S^+_{\mathbf{R}}\rangle=\frac{1}{N}\sum_{\mathbf{q}}C_{\mathbf{q}}\mathrm{e}^{i\mathbf{qR}}, \tag{12}$$

where $\mathbf{R}=n\mathbf{a}_x+m\mathbf{a}_y$. The GMFA spectrum (10) is calculated self-consistently by using the MFA approximation for the static correlation function (12),

$$C_{\mathbf{q}}=\frac{m(\mathbf{q})}{2\,\omega_{\mathbf{q}}}\,\coth\frac{\beta\,\omega_{\mathbf{q}}}{2}\,. \tag{13}$$

The decoupling parameters α_1,α_2 and λ_1,λ_2 in Eq. (10) take into account the vertex renormalization for the spin–spin and electron–spin interaction, respectively, as explained in [24]. In particular, the parameters α_1,α_2 are evaluated from the results for the Heisenberg model at $\delta=0$ and are kept fixed for $\delta\neq 0$. The parameters λ_1,λ_2 are calculated from the sum rule $C_{0,0}=\langle S^+_0S^-_0\rangle=(1/2)(1-\delta)$ with a fixed ratio $\lambda_1/\lambda_2=0.378$. In the superconducting state, the electron

correlation function $F_{\mathbf{R}}$ is calculated by the spectral function for electrons in the superconducting state (see Eq. (22)). The variation of the parameters λ_1, λ_2 below the superconducting transition is negligibly small and practically has no influence on the spectrum $\omega_{\mathbf{q}}$.

The direct calculation of $m(\mathbf{q})$ yields

$$m(\mathbf{q}) = -8(1-\gamma_{\mathbf{q}})\left[t\,F_{1,0} + J\,C_{1,0}\right]. \tag{14}$$

Thus, the static susceptibility (8) is explicitly determined by Eqs. (10) and (14).

2.3. Self-Energy. In what follows, we consider the t–J model at a finite hole doping $\delta > 0.05$ when, as discussed in [24], the largest contribution to the self-energy (4) is $\Sigma_t(\mathbf{q},\omega)$ coming from the spin–electron scattering. It is determined by the hopping term H_t in the t–J model according to the equation for the spin-density operators: $-\ddot{S}^{\pm}_{\mathbf{q}} = [[S^{\pm}_{\mathbf{q}}, H_t], H_t]$. As described in Appendix, in the MCA this contribution reads

$$\begin{aligned}
&\Sigma''_t(\mathbf{q},\omega) = -\frac{\pi(2t)^4(e^{\beta\omega}-1)}{m(\mathbf{q})\,\omega}\int\int\int_{-\infty}^{\infty} d\omega_1 d\omega_2 d\omega_3 \\
&\frac{1}{N^2}\sum_{\mathbf{q_1},\mathbf{q_2}} N(\omega_2)[1-n(\omega_1)]n(\omega_3)\delta(\omega+\omega_1-\omega_2-\omega_3) \\
&B_{\mathbf{q_2}}(\omega_2)\big[(\Lambda^2_{\mathbf{q_1},\mathbf{q_2},\mathbf{q_3}} + \Lambda^2_{\mathbf{q_3},\mathbf{q_2},\mathbf{q_1}})\,A^N_{\mathbf{q_1}}(\omega_1)\,A^N_{\mathbf{q_3}}(\omega_3) \\
&-2\Lambda_{\mathbf{q_1},\mathbf{q_2},\mathbf{q_3}}\Lambda_{\mathbf{q_3},\mathbf{q_2},\mathbf{q_1}}\,A^S_{\mathbf{q_1}\sigma}(\omega_1)\,A^S_{\mathbf{q_3}\sigma}(\omega_3)\big],
\end{aligned} \tag{15}$$

where $\mathbf{q}_3 = \mathbf{q} - \mathbf{q}_1 - \mathbf{q}_2$. The Fermi and Bose functions are denoted by $n(\omega) = (e^{\beta\omega}+1)^{-1}$ and $N(\omega) = (e^{\beta\omega}-1)^{-1}$. The vertex function $\Lambda_{\mathbf{q_1},\mathbf{q_2},\mathbf{q_3}}$ is defined by Eq. (31). Here we introduced the spectral functions:

$$A^N_{\mathbf{q}}(\omega) = -(1/\pi)\mathrm{Im}\langle\langle X^{0\sigma}_{\mathbf{q}} | X^{\sigma 0}_{\mathbf{q}}\rangle\rangle_{\omega}, \tag{16}$$

$$A^S_{\mathbf{q}\sigma}(\omega) = -(1/\pi)\mathrm{Im}\langle\langle X^{0\sigma}_{\mathbf{q}} | X^{0\bar{\sigma}}_{-\mathbf{q}}\rangle\rangle_{\omega}, \tag{17}$$

$$B_{\mathbf{q}}(\omega) = (1/\pi)\,\chi''(\mathbf{q},\omega), \tag{18}$$

where $A^{N,S}_{\mathbf{q}}(\omega)$ are determined by the retarded anticommutator GFs for electrons (see [25]). In comparison with the expression for the self-energy in the normal state considered in [24], in Eq. (15) there is the contribution proportional to the anomalous GF $\langle\langle X^{0\sigma}_{\mathbf{q}} | X^{0\bar{\sigma}}_{-\mathbf{q}}\rangle\rangle_{\omega}$ which is nonzero in the superconducting state only.

It should be emphasized that the self-energy (15) is determined by the decay of a spin excitation with the energy ω and wave vector $\mathbf{q}$ into three excitations: a particle–hole pair and a spin excitation. This process is controlled by the energy and momentum conservation laws, $\omega = (\omega_3 - \omega_1) + \omega_2$ and $\mathbf{q} = \mathbf{q}_1 + \mathbf{q}_2 + \mathbf{q}_3$, respectively. In the previous studies of the t–J model the contribution of the additional spin excitation has been neglected (see, e.g., [15]) or approximated

by static or mean-field-type expressions (see, e.g., [17] and [21]). That is, in these approximations the spin-excitation contribution was «decoupled» from the particle–hole pair. We can derive the particle–hole bubble approximation from Eq. (15), if we ignore the spin-energy contribution ω_2 in comparison with the electron–hole pair energy, or, equivalently, if in the MCA, Eqs. (32) and (33), the time-dependent spin correlation function is approximated by its static value: $\langle S^-_{-\mathbf{q}} S^+_{\mathbf{q}}(t)\rangle \simeq \langle S^-_{-\mathbf{q}} S^+_{\mathbf{q}}\rangle = C_{\mathbf{q}}$. Moreover, excluding the spin-excitation wave vector $\mathbf{q}_2$ from the wave-vector conservation law, we have $\mathbf{q} = \mathbf{q}_1 + \mathbf{q}_3$. As a result of these approximations in Eq. (15), we obtain the self-energy in the form of the particle–hole bubble approximation:

$$\widetilde{\Sigma}''_t(\mathbf{q},\omega) = -\frac{\pi(2t)^4}{m(\mathbf{q})\,\omega}\int_{-\infty}^{\infty} d\omega_1[n(\omega_1) - n(\omega_1+\omega)]\times$$
$$\times\,\frac{1}{N}\sum_{\mathbf{q_1}}\big[\widetilde{\Lambda}^N_{\mathbf{q_1},\mathbf{q}-\mathbf{q_1}}\,A^N_{\mathbf{q_1}}(\omega_1)\,A^N_{\mathbf{q}-\mathbf{q_1}}(\omega_1+\omega) -$$
$$-\,\widetilde{\Lambda}^S_{\mathbf{q_1},\mathbf{q}-\mathbf{q_1}}\,A^S_{\mathbf{q_1}\sigma}(\omega_1)\,A^S_{\mathbf{q}-\mathbf{q_1}\sigma}(\omega_1+\omega)\big], \quad (19)$$

where the averaged over the spin-excitation wave vector $\mathbf{q_2}$ vertexes are introduced,

$$\widetilde{\Lambda}^N_{\mathbf{q_1},\mathbf{q_3}} = \frac{1}{N}\sum_{\mathbf{q_2}} C_{\mathbf{q}_2}[\Lambda^2_{\mathbf{q_1},\mathbf{q_2},\mathbf{q_3}} + \Lambda^2_{\mathbf{q_3},\mathbf{q_2},\mathbf{q_1}}], \quad (20)$$

$$\widetilde{\Lambda}^S_{\mathbf{q_1},\mathbf{q_3}} = \frac{2}{N}\sum_{\mathbf{q_2}} C_{\mathbf{q}_2}\Lambda_{\mathbf{q_1},\mathbf{q_2},\mathbf{q_3}}\Lambda_{\mathbf{q_3},\mathbf{q_2},\mathbf{q_1}}. \quad (21)$$

In the approximation (19) only the opening of a superconducting gap in the particle–hole excitation can suppress the damping of spin excitations due to the decay into particle–hole pairs which may result in the RM. Below we discuss in more detail why a particle–hole bubble approximation for the self-energy (19) leads to a different behavior of the spin-excitation damping in comparison with the results obtained for the full self-energy (15).

3. RESULTS AND DISCUSSION

3.1. Self-Energy Approximation. In the calculation of the self-energy (15) we adopt the mean-field approximation (MFA) for the electron spectral functions (16) and (17) which in the superconducting state can be written as

$$A^N_{\mathbf{q}}(\omega) = Q\sum_{\omega_1=\pm E_{\mathbf{q}}}\frac{\omega_1+\varepsilon_{\mathbf{q}}}{2\omega_1}\delta(\omega-\omega_1), \quad (22)$$

$$A^S_{\mathbf{q}\sigma}(\omega) = Q \sum_{\omega_1=\pm E_{\mathbf{q}}} \frac{\Delta_{\mathbf{q}\sigma}}{2\omega_1}\delta(\omega-\omega_1). \tag{23}$$

Here $Q = 1 - n/2$ is the Hubbard weighting factor and the superconducting gap function $\Delta_{\mathbf{q}\sigma} = (\mathrm{sgn}\ \sigma)\Delta_{\mathbf{q}}$. In the electron spectrum $\varepsilon_{\mathbf{q}}$ we take into account only the nearest-neighbor hopping t and consider the energy dispersion in the Hubbard-I approximation: $\varepsilon_{\mathbf{q}} = -4t\,Q\,\gamma_{\mathbf{q}} - \mu$. The spectrum of quasiparticles in the superconducting state is given by the conventional formula $E_{\mathbf{q}} = \sqrt{\varepsilon^2_{\mathbf{q}} + \Delta^2_{\mathbf{q}}}$. For the spin-excitation spectral function (18) we take the form:

$$B_{\mathbf{q}}(\omega) = m(\mathbf{q}) \sum_{\omega_1=\pm\widetilde{\omega}_{\mathbf{q}}} \frac{1}{2\omega_1}\delta(\omega-\omega_1), \tag{24}$$

where the spectrum of spin excitations $\widetilde{\omega}_{\mathbf{q}}$ is determined by the pole of the DSS, $\widetilde{\omega}_{\mathbf{q}} = [\omega^2_{\mathbf{q}} + \widetilde{\omega}_{\mathbf{q}}\,\Sigma'(\mathbf{q},\widetilde{\omega}_{\mathbf{q}})]^{1/2}$. Here, the real part of the self-energy $\Sigma'(\mathbf{q},\omega)$ is calculated perturbationally by taking the spectral function (24) with the GMFA spectrum $\omega_1 = \pm\omega_{\mathbf{q}}$. Using these spectral functions, after integration over the energies in Eq. (15) we write the imaginary part of the self-energy in the following form convenient for the calculation in the limit $T \to 0$:

$$\begin{aligned}
\Sigma''_t(\mathbf{q},\omega) = {} & \frac{\pi(2t)^4}{\omega m(\mathbf{q})}\frac{Q^2}{N^2}\sum_{\mathbf{q_1},\mathbf{q_2}}\sum_{\omega_1=\pm E_{\mathbf{q}_1}}\sum_{\omega_2=\pm\widetilde{\omega}_{\mathbf{q}_2}}\sum_{\omega_3=\pm E_{\mathbf{q}_3}} \\
& m(\mathbf{q}_2)\frac{N(\omega_2)n(-\omega_1)n(\omega_3) + N(-\omega_2)n(\omega_1)n(-\omega_3)}{8\omega_1\omega_2\omega_3} \\
& \big[(\Lambda^2_{\mathbf{q_1},\mathbf{q_2},\mathbf{q_3}} + \Lambda^2_{\mathbf{q_3},\mathbf{q_2},\mathbf{q_1}})(\omega_1+\varepsilon_{\mathbf{q}_1})(\omega_3+\varepsilon_{\mathbf{q}_3}) \\
& - 2\Lambda_{\mathbf{q_1},\mathbf{q_2},\mathbf{q_3}}\Lambda_{\mathbf{q_3},\mathbf{q_2},\mathbf{q_1}}\Delta_{\mathbf{q}_1}\Delta_{\mathbf{q}_3}\big]\delta(\omega+\omega_1-\omega_2-\omega_3).
\end{aligned} \tag{25}$$

Similar calculations for the self-energy (19) in the particle–hole bubble approximation yield

$$\begin{aligned}
\widetilde{\Sigma}''_t(\mathbf{q},\omega) = {} & -\frac{\pi(2t)^4}{m(\mathbf{q})\omega}\frac{Q^2}{N}\sum_{\mathbf{q_1}}\sum_{\omega_1=\pm E_{\mathbf{q}_1}}\sum_{\omega_2=\pm E_{\mathbf{q}-\mathbf{q}_1}} \\
& \frac{n(\omega_1)-n(\omega_2)}{4\omega_1\omega_2}\big[\widetilde{\Lambda}^N_{\mathbf{q_1},\mathbf{q}-\mathbf{q_1}}(\omega_1+\varepsilon_{\mathbf{q}_1})(\omega_2+\varepsilon_{\mathbf{q}-\mathbf{q}_1}) \\
& - \widetilde{\Lambda}^S_{\mathbf{q_1},\mathbf{q}-\mathbf{q_1}}\Delta_{\mathbf{q}_1}\Delta_{\mathbf{q}-\mathbf{q}_1}\big]\,\delta(\omega+\omega_1-\omega_2).
\end{aligned} \tag{26}$$

We consider both the d-wave and s-wave symmetry of the superconducting gap which we write as $\Delta^{(d)}_{\mathbf{q}} = (\Delta/2)(\cos q_x - \cos q_y)$ and $\Delta^{(s)} = \Delta$ with the temperature-dependent amplitude $\Delta(T)$. In numerical calculations we assume

that $\Delta(T)$ follows the conventional Bardeen–Cooper–Schrieffer (BCS) theory. In particular, $\Delta(T)/k_{\rm B}T_{\rm c} = 1.76, 1.72, 1.6, 1.24$ for $T/T_{\rm c} = 0, 0.4, 0.6, 0.8$, respectively. By taking, instead of the BCS ratio $2\Delta_0/k_{\rm B}T_{\rm c} = 3.52$, $\Delta_0 = \Delta(T=0)$, the ratio $2\Delta_0/k_{\rm B}T_{\rm c} = 4.3$ for a pure d-wave superconductor (see, e.g., [27]) we have found that the results do not change noticeably, i.e., less than 5% at $T = 0$ and even less at finite temperatures. We mainly consider two doping values, $\delta = 0.2$ which is larger than optimal doping and $\delta = 0.09$ for the underdoped case. For $\delta = 0.2$ we fix the superconducting transition temperature as $k_{\rm B}T_{\rm c} = 0.025t$, while for $\delta = 0.09$ we take $k_{\rm B}T_{\rm c} = 0.016t$. For the hopping parameter $t = 0.313$ eV these values are close to $T_{\rm c} = 91$ K in the nearly optimally doped $YBCO_{6.92}$ single crystal in [1] and $T_{\rm c} = 59$ K in the underdoped ($\delta = 0.09$) $YBCO_{6.5}$ crystal studied in [6]. We take the exchange interaction $J = 0.3\,t$ and measure all energies in unit of t.

3.2. Spin-Excitation Damping. To elucidate the role of spin excitations in the damping and their relevance to the shape of the spectral function, Eq. (7), we consider the temperature dependence of the spin-excitation damping at the AF wave vector, $\Gamma(\mathbf{Q},\omega) = -(1/2)\,\Sigma_t''(\mathbf{Q},\omega)$. Figure 1 shows the damping for $\delta = 0.2$ at various temperatures in the case of the d-wave (*a*) and s-wave (*b*) pairing. The difference of the damping appears only at low ω and T. In particular, the damping for the s-wave gap at $T = 0$ disappears at $\omega < 2\Delta_0 \simeq 4k_{\rm B}T_{\rm c} = 0.1t$, while for the d-wave gap it vanishes at $\omega \simeq \Delta_0 \simeq 0.05t$. A weak damping was obtained also for the normal state shown in Fig. 1, *c* when the contribution from the superconducting gap functions in the self-energy $\Sigma_t''(\mathbf{Q},\omega)$, Eq. (25), is omitted. The similar smooth variation of the damping with energy in all three cases below $T_{\rm c}$, contrary to a step-like dependence obtained in the particle–hole bubble approximation (see below), demonstrates that the superconducting gap plays a minor role in suppressing the damping, and the gap $\widetilde{\omega}_{\mathbf{Q}}$ in the spin-excitation spectrum is responsible for such a peculiar behavior. For a lower doping, the damping becomes an order of magnitude weaker as shown in Fig. 2 at $\delta = 0.09$, even above $T_{\rm c}$ ($T = 1.4T_{\rm c}$).

Sometimes, the RM observed above $T_{\rm c}$ in the underdoped cuprates is related to a pseudogap in the electronic spectrum (see, e.g., [3]). We propose another explanation: The RM above $T_{\rm c}$ is the result of the gapped spin excitations in the self-energy (25) leading to a very weak damping in the underdoped region which is outlined in more detail below. This explanation is supported by studies of the spin-excitation damping $\Gamma_{\mathbf{q}} = -(1/2)\,\Sigma_t''(\mathbf{q},\omega = \widetilde{\omega}_{\mathbf{q}})$ at $T = 0$ shown in Fig. 3. The small difference between the damping in the d-wave superconducting state and the normal state observed for the full self-energy, Eq. (25), confirms that the superconducting gap does not play an essential role in suppressing the damping $\Gamma_{\mathbf{Q}}$, in particular, in the underdoped region. At the same time, the sharp increase of $\Gamma_{\mathbf{q}}$ away from the AF wave vector $\mathbf{Q}$ explains the resonance character of spin excitations at $\mathbf{Q}$.

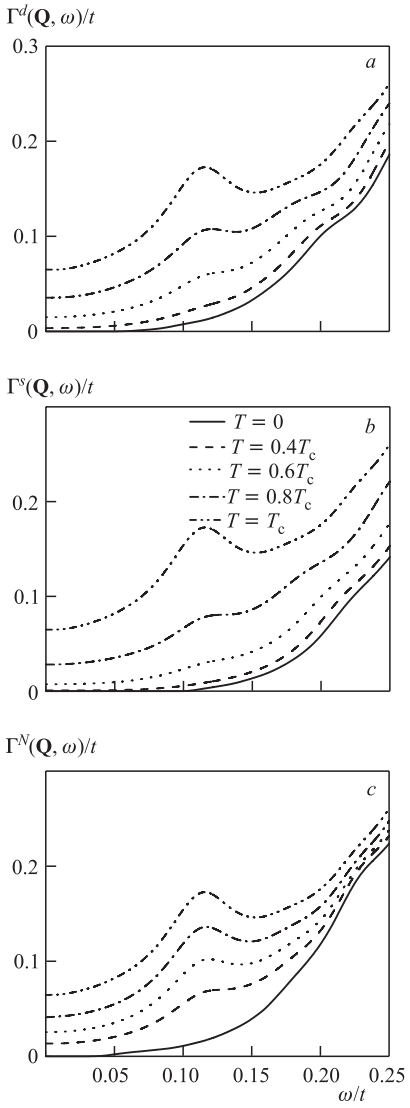

Fig. 1. Spin-excitation damping $\Gamma(\mathbf{Q},\omega)$ for $\delta = 0.2$ at $T \leqslant T_c$ for *a*) the d-wave and *b*) s-wave pairing, and *c*) in the normal state

Though the damping in Fig. 1 looks similar, the spectral functions shown in Fig. 4 for $\delta = 0.2$ at $T = 0.4T_c$ reveal a strong enhancement of the intensity of the RM in the superconducting state. In comparison to the normal state, where

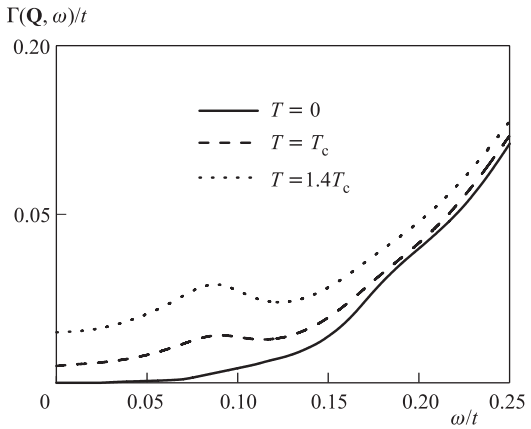

Fig. 2. Spin-excitation damping $\Gamma(\mathbf{Q}, \omega)$ for $\delta = 0.09$ at $T \leqslant T_{\rm c}$ for the d-wave pairing

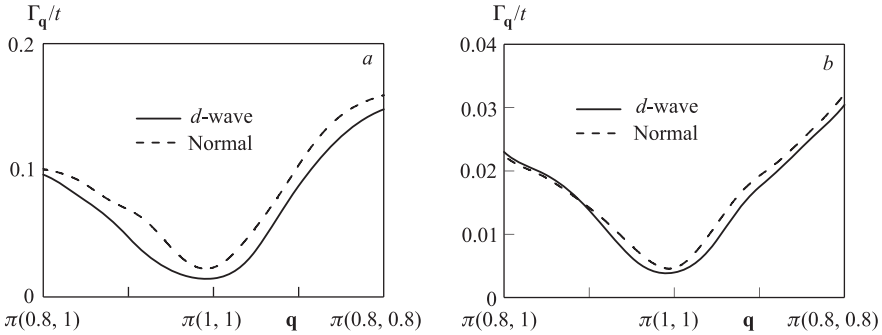

Fig. 3. Spin-excitation damping $\Gamma_{\mathbf{q}}$ for *a*) $\delta = 0.2$ and for *b*) $\delta = 0.09$ at $T = 0$ for the d-wave pairing (solid line) and in the normal state (dashed line)

the contribution from the superconducting gap is omitted, the peak intensity is about two (five) times larger for the $d\,(s)$-wave symmetry of the gap.

Quite a different behavior of the damping and the spectral function is obtained for the reduced self-energy, Eq. (26), with a contribution only from a particle–hole bubble. Figure 5 shows our results for the spectral function $\chi''(\mathbf{q}, \omega)$ and for the damping $\Gamma(\mathbf{Q}, \omega)$. To compare these functions with those calculated in [17], we adopt the electron dispersion used in [17], $\varepsilon_{\mathbf{q}}^{\rm eff} = -4\, t_{\rm eff}\gamma_{\mathbf{q}} - 4\, t'_{\rm eff}\, \cos q_x\, \cos q_y$ with $t_{\rm eff} = 0.3t$ and $t'_{\rm eff} = -0.1t$ and take the gap parameter $\Delta_0 = 0.1t$. The obtained results are quite close to those shown in Fig. 1 of [17] (where $\chi''_{zz}(\mathbf{q}, \omega) = (1/2)\chi''(\mathbf{q}, \omega)$ is plotted). At $T = 0$, we observe a much narrower RM, but with a lower intensity in comparison with the RM calculated with the

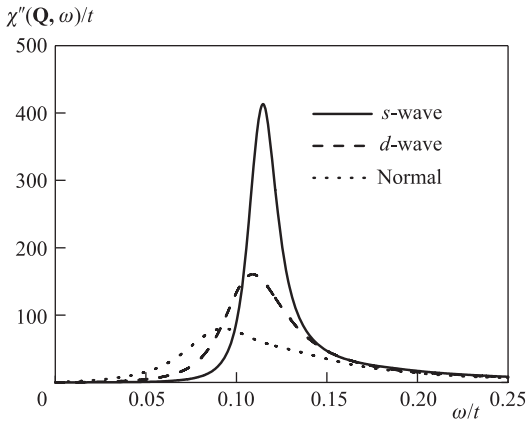

Fig. 4. Spectral function $\chi''(\mathbf{Q},\omega)$ for the d-wave and s-wave pairing in comparison with the normal state at $T = 0.4T_c$ for $\delta = 0.2$

full self-energy, Eq. (25), as shown in Fig. 6. The energy E_r of the RM shown Fig. 5, *a* noticeably decreases with increasing temperature, contrary to a negligible shift of the RM shown in Fig. 6 for $T = 0.4T_c$. This comparison demonstrates that in the particle–hole bubble approximation the superconducting gap plays a crucial role in the occurrence of the RM with $E_r(T) < 2\Delta(T)$, while in the full self-energy (25) the superconducting gap and details of the electron dispersion are less important. In particular, for the underdoped case $\delta = 0.09$ we have not found visible changes of the damping function shown in Fig. 2 for the electron dispersion with $t' = 0$ and $t' = -0.1t$. For the reduced self-energy, Eq. (26), the damping vanishes for both types of the dispersion in the underdoped region, and in order to obtain a finite damping at $\delta = 0.1$ in [17] (see Fig. 2), the authors have to use the electron density of states in the damping function (see their Eq. (20)) instead of the $\mathbf{q}$-dependent electron spectral functions.

This difference can be explained as follows. Whereas in the particle–hole bubble approximation given by Eq. (26) the spin excitation with the energy ω at the wave vector $\mathbf{Q}$ can decay only into a particle–hole pair with the energy $\omega(\mathbf{Q}) = E_{\mathbf{Q}+\mathbf{q}}+E_{\mathbf{q}}$, in a more general process described by Eq. (25) an additional spin excitation participates in the scattering. In the limit $T \to 0$, the decay process in this case is governed by another energy-conservation law, $\omega(\mathbf{Q}) = E_{\mathbf{q_3}}+E_{\mathbf{q_1}}+\widetilde{\omega}_{\mathbf{q_2}}$ where the largest contribution from the spin excitation comes from $\widetilde{\omega}_{\mathbf{q_2}} \simeq \widetilde{\omega}_{\mathbf{Q}}$ due to the factor $m_{\mathbf{q_2}}$ (14) in Eq. (25). This energy-momentum conservation law strongly reduces the phase space for the decay and suppresses the damping of the initial spin excitation with the energy $\omega(\mathbf{Q})$. In fact, the occurrence of an additional spin excitation in the scattering process with the finite energy $\widetilde{\omega}_{\mathbf{Q}}$ plays a role similar to the superconducting gap in the excitation of the particle–hole

pair in Eq. (26). Therefore, the damping at low temperatures ($k_{\rm B}\,T \ll \widetilde{\omega}_{\mathbf{Q}} \sim E_{\rm r}$) appears to be small even in the normal state as demonstrated in Fig. $1,c$. In the case of the particle–hole relaxation, the condition for the occurrence of the RM, $\omega(\mathbf{Q}) = E_{\mathbf{q}+\mathbf{Q}} + E_{\mathbf{q}} \leq 2\Delta(\mathbf{q}^*)$, imposes a strong restriction on the shape of the FS which should cross the AF Brillouin zone to accommodate the scattering vector $\mathbf{Q}$ and the vector $\mathbf{q}^*$ on the FS. In the case of the full self-energy, Eq. (25), the energy-momentum conservation law for three quasipartricles does not impose such strong limitations.

3.3. Resonance Mode. Experimentally, the RM energy $E_{\rm r}$ decreases with underdoping following the superconducting transition temperature, $E_{\rm r} \simeq 5.3 k_{\rm B} T_{\rm c}$, but only weakly depends on temperature (see, e.g., [2, 3]). Now we discuss the temperature and doping dependence of the RM and its dispersion within our theory for the d-wave pairing.

The temperature dependence of the spectral function in the overdoped case $\delta = 0.2$ is shown in Fig. 6. It has high intensity at low temperatures, but strongly decreases with temperature and becomes very broad at $T \sim T_{\rm c}$ as found in experiments (see [1]). In Fig. 7 the temperature dependence of the spectral function for the underdoped case $\delta = 0.09$ is plotted. Whereas the resonance energy decreases with underdoping, the intensity of the RM greatly increases in accordance with experiments. The RM energy weakly depends on temperature and is still quite visible at $T = T_{\rm c}$ and even at $T = 1.4 T_{\rm c}$.

The dispersion of the spectral function for $\delta = 0.2$ is shown in Figs. 8 and 9. A strong suppression of the spectral-function intensity away from $\mathbf{Q} = \pi(1, 1)$ even at $T = 0$ explains the resonance-type behavior of the function at low temperatures. This suppression of the intensity is in accord with the sharp increase of the damping away from $\mathbf{Q}$ shown in Fig. 3.

We have not found the downward dispersion at energies below the RM detected in neutron-scattering experiments on $YBCO_{6.5}$ ([7]). However, as argued in [7], two distinct regions of spin excitations may be suggested: a low-energy part below $E_{\rm r} \approx 33$ meV, which can be described as incommensurate stripe-like collective spin excitations for the acoustic mode, and a high-energy part, which has a spin-wave character. The high-energy part of the spin excitations has an isotropic in-plane dispersion while the low-energy excitations show a one-dimensional character. The different nature of the two parts of the spectrum is also revealed in their temperature dependence: the low-energy acoustic part of the spectrum is strongly influenced by the superconducting transition, while the high-energy part of the spectrum does not change appreciably with temperature up to 85 K. Nevertheless, in several theoretical models the downward dispersion of the lower-energy part of the spectrum was reproduced in the RPA approach (see, e.g., [9]) or, for the $t-J$ model, within the particle–hole bubble approximation (see [15, 19, 21]). The dispersion was explained by a special wave-vector dependence of the particle–hole bubble diagram related to the wave-vector dependence

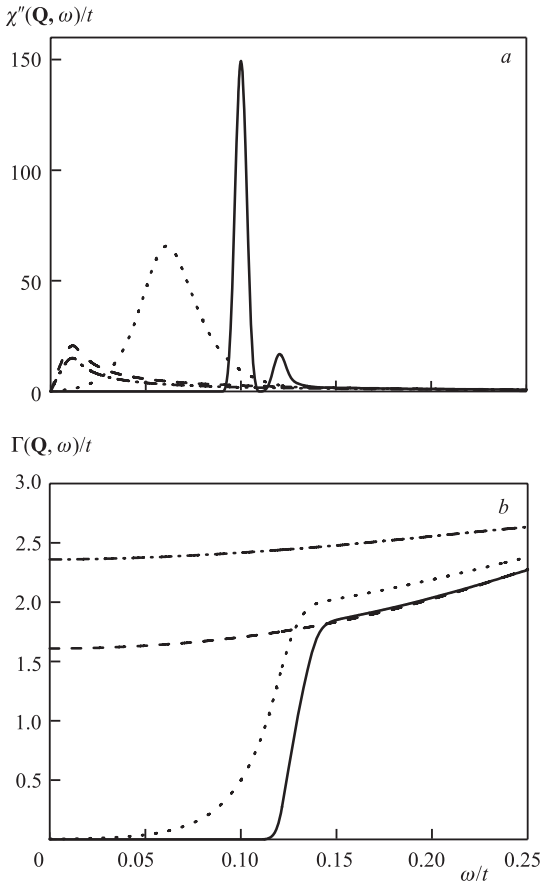

Fig. 5. *a*) Spectral function $\chi''(\mathbf{Q},\omega)$ and *b*) spin-excitation damping $\Gamma(\mathbf{Q},\omega)$ calculated in the particle–hole bubble approximation, Eq. (19), at $\delta = 0.2$ for the d-wave pairing ($\Delta_0 = 0.1t$ taken from [17]) at $T = 0$ (solid line) and $T = 0.4T_{\rm c}$ (dotted line), and for the normal state at $T = 0$ (dashed line) and $T = T_{\rm c}$ (dash-dotted line)

of the $d_{x^2-y^2}$ superconducting gap and to a specific for cuprates two-dimensional FS. Since in our theory beyond the RPA the RM energy does not critically depend on specific properties of the FS and the superconducting gap, the downward dispersion cannot be found. To discuss this problem in detail, the role of stripe excitations in the spin-excitation spectrum should be elucidated.

Now we discuss the doping dependence of the RM energy $E_{\rm r}(\delta)$. At low temperatures, the real part of the self-energy $\Sigma'(\mathbf{Q},\omega) < 0$ is quite large as shown in Fig. 10. This considerably softens the energy of spin excitations $\omega_{\mathbf{Q}}$

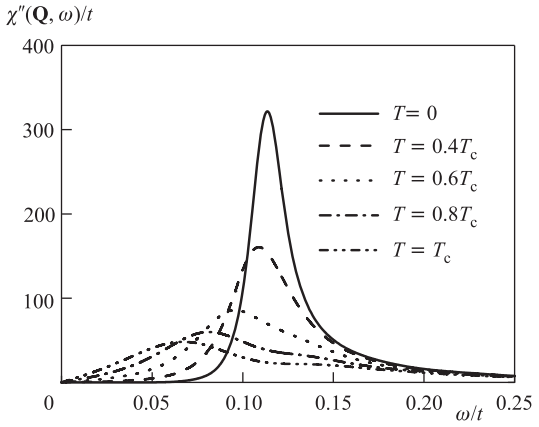

Fig. 6. Temperature dependence of the spectral function $\chi''(\mathbf{Q},\omega)$ at $\delta = 0.2$

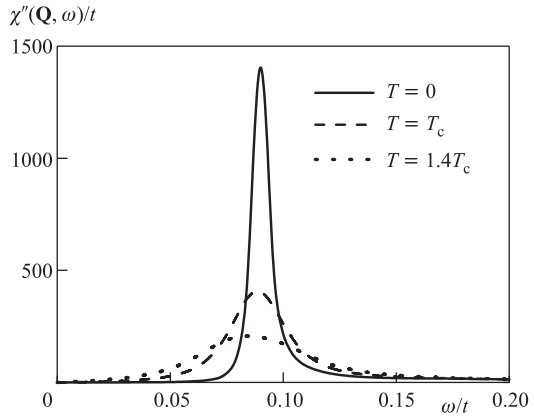

Fig. 7. Temperature dependence of the spectral function $\chi''(\mathbf{Q},\omega)$ at $\delta = 0.09$

in the GMFA, Eq. (10), shifting the pole of the spectral function $\chi''(\mathbf{Q},\omega)$ to a lower energy: $\widetilde{\omega}_{\mathbf{Q}} = [\omega_{\mathbf{Q}}^2 - \widetilde{\omega}_{\mathbf{Q}}\,|\Sigma'(\mathbf{Q},\widetilde{\omega}_{\mathbf{Q}})|]^{1/2}$. Experimentally, the RM energy is measured by the position $E_{\rm r}$ of the maximum in the spectral function $\chi''(\mathbf{Q},\omega)$ which deviates from $\widetilde{\omega}_{\mathbf{Q}}$ due to a finite width of excitations. In Fig. 11 the doping dependence $E_{\rm r}(\delta)$ in the superconducting state at $T = 0$ determined by the maximum of the spectral function is plotted. Thereby, for the doping dependence of $\Delta_0(\delta) = 1.76\,T_{\rm c}(\delta)$ we used the universal empirical formula $T_{\rm c}(\delta) = T_{\rm c,max}\,[1 - \beta\,(\delta - \delta_{\rm opt})^2]$ [28], where $\delta_{\rm opt} = 0.16$, $T_{\rm c,max} = 93$ K, and

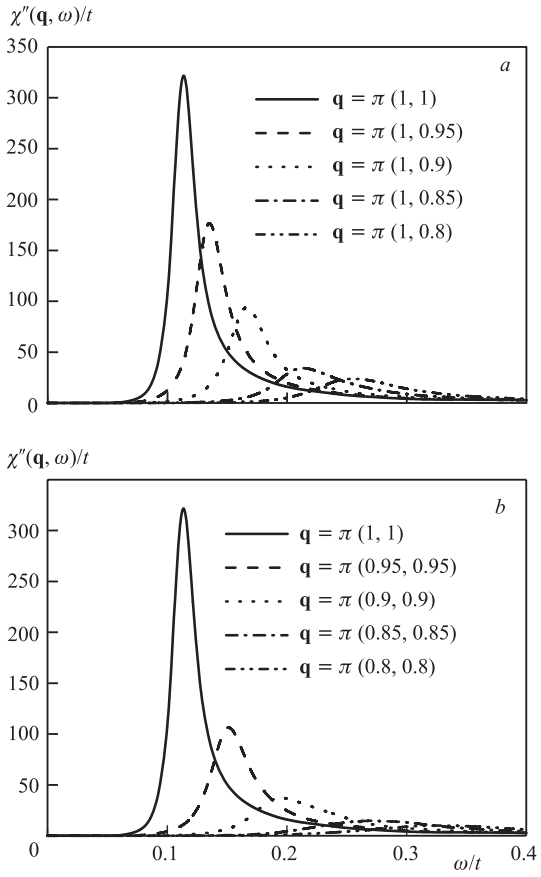

Fig. 8. Spectral function $\chi''(\mathbf{q},\omega)$ for the wave vectors: *a*) $\mathbf{q}=\pi(1,\xi)$ and *b*) $\mathbf{q}=\pi(\xi,\xi)$ at $T=0$ for $\delta=0.2$

the value of $\beta=75$ was fitted to obtain $T_c=59$ K for $\delta=0.09$ in $YBCO_{6.5}$, [6]. With decreasing δ, E_r decreases which qualitatively agrees with the experimental data. The energy of the RM tends to zero at the critical doping $\delta_c=0.038$ below which the long-range AF order emerges at $T=0$, as we have shown in [24]. So, in our scenario the RM is just the soft mode which brings about the long-range AF order below the critical doping. Experimentally, in the overdoped region the RM energy decreases with increasing doping (see Fig. 11 and, e.g., [12]), while in our theory E_r tends to increase due to the increasing energy $\widetilde{\omega}_{\mathbf{Q}}$. However, as shown in [24], the damping in the overdoped region rapidly increases and the RM becomes overdamped. Note for $\delta\lesssim 0.2$, the magnitude of E_r agrees well

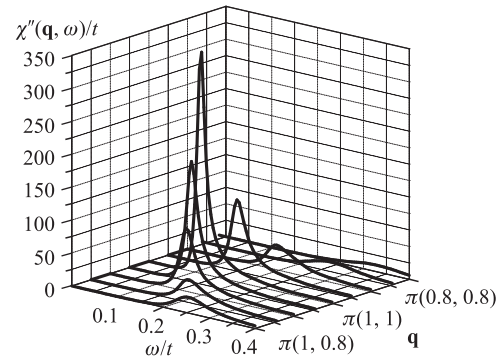

Fig. 9. Spectral function $\chi''(\mathbf{q}, \omega)$ near the wave vector $\mathbf{Q} = \pi(1, 1)$ at $T = 0$ for $\delta = 0.2$

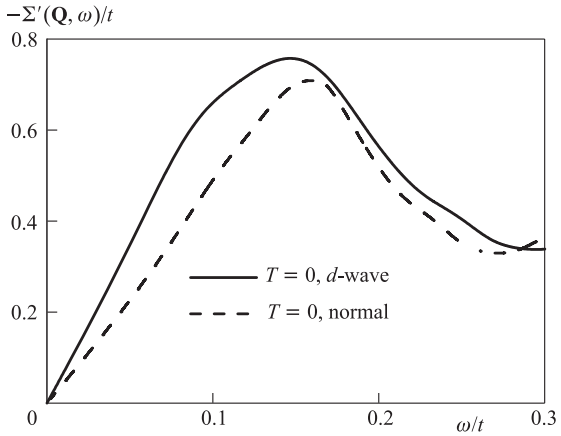

Fig. 10. Real part of the self-energy $\Sigma'(\mathbf{Q}, \omega)$ for the d-wave pairing in comparison with the normal state at $T = 0$ for $\delta = 0.2$

with experiments, where in the approach of [17] a too large superconducting gap $\Delta_0 \sim 0.1t$ (compare with Fig. 5) has to be taken to fit the RM energy to the experimentally observed one.

In Fig. 12 we compare our results with the neutron-scattering data for the nearly optimally doped $YBCO_{6.92}$ single crystal [1] at $T = 5$ K and $T = 100$ K. In this sample, $T_c = 91$ K and the RM energy $E_r \simeq 40$ meV$= 5.1 k_B T_c > 2\,\Delta_0$ (taking $2\Delta_0(\delta) = 3.52\, k_B T_c(\delta)$ we have $E_r \simeq 2.9\Delta_0$). For $\delta = 0.2$, our calculations yield $E_r = 0.12t = 38$ meV$= 4.8 k_B T_c = 2.7\,\Delta_0$ ($t = 0.313$ eV, $T_c = 0.025t$; see Subsec. 3.1).

In Fig. 13 our results are compared with the experimental data for the underdoped ortho-II $YBCO_{6.5}$ single crystal with $E_r = 33$ meV$= 6.5\, k_B T_c = 3.7\,\Delta_0$

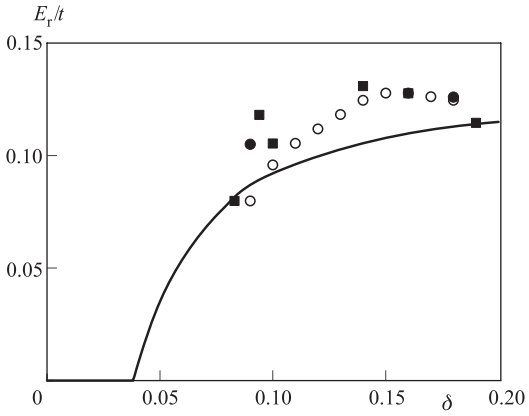

Fig. 11. Energy of the resonance mode $E_{\rm r}$ at $T = 0$ as a function of hole doping δ in comparison with experimental data for YBCO from [2] (open circles), [3] (full squares), and [1], [6] (full circles)

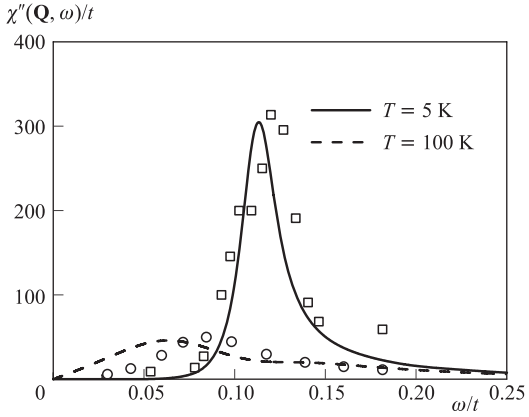

Fig. 12. Spectral function $\chi''(\mathbf{Q},\omega)$ for doping $\delta = 0.2$ compared to experimental data for $YBCO_{6.92}$ [1], at $T = 5$ K (squares) and $T = 100$ K (circles)

at $T = 8$ K and $T = 85$ K (see Fig. 14 in [6]). For $\delta = 0.09$, our theory gives $E_{\rm r} = 0.09t = 28$ meV$= 5.6\, k_{\rm B}\, T_{\rm c} = 3.2\, \Delta_0$. We note a weak temperature dependence of the RM energy observed experimentally and obtained in our calculation. In both compounds the RM energy is larger than the superconducting excitation energy, $E_{\rm r} > 2\Delta_0$, while in the spin-1 exciton scenario the RM energy $E_{\rm r}$ has to be less than $2\Delta_0$. So we obtain a good agreement of our theory with neutron-scattering experiments on YBCO crystals both near the optimal doping and in the underdoped region.

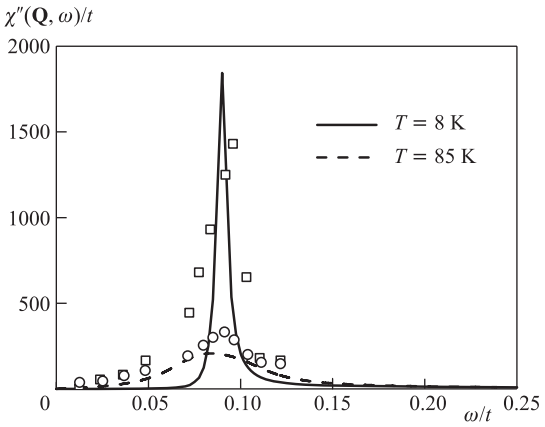

Fig. 13. Spectral function $\chi''(\mathbf{Q},\omega)$ for doping $\delta = 0.09$ compared to experimental data for $YBCO_{6.5}$ [6], at $T = 8$ K (squares) and $T = 85$ K (circles)

CONCLUSION

A detailed study of the DSS in the superconducting state has revealed the important role of the spin-excitation damping in the RM phenomenon. We have found that the low-temperature damping essentially depends on the gap $\widetilde{\omega}_{\mathbf{Q}} \simeq E_{\rm r}$ in the spin-excitation spectrum at the AF wave vector $\mathbf{Q}$, while an opening of a superconducting gap $2\Delta(T)$ below $T_{\rm c}$ is less important. Since the energy of the RM $E_{\rm r} \sim 5\,k_{\rm B}T_{\rm c}$ does not show temperature dependence, at $T \lesssim T_{\rm c}$, the spin gap at $E_{\rm r}$ plays the dominant role in the suppression of damping, since the superconducting energy $2\Delta(T \lesssim T_{\rm c}) \ll E_{\rm r}$. This follows from Eq. (25) for the self-energy, where in the decay of a spin excitation, besides a particle–hole pair, the contribution from an additional spin excitation is taken into account. This is in contrast to the particle–hole bubble approximation in Eq. (26) which is used in the RPA (see, e.g., [9,15]) and in similar approximations in memory-function theories [17,19,21]. In those approximations, the spin-excitation damping is much larger in the normal state and reveals a spin gap only at $T \ll T_{\rm c}$, where the RM appears (see Fig. 5). The gapped spin-excitation spectrum in the full self-energy (25) greatly suppresses the damping at $T = 0$ which results in a comparable damping both in the superconducting state (either of d-wave or s-wave symmetry) and in the normal state, as demonstrated in Figs. 1 and 3. The damping is strongly decreasing in the underdoped region (see Figs. 2 and 3) bringing about a much stronger RM seen also above $T_{\rm c}$ (Fig. 7).

With decreasing hole concentration the energy of the RM decreases and shows the dependence close to that observed in neutron-scattering experiments, $E_{\rm r} \sim 5k_{\rm B}T_{\rm c}$ (see Fig. 11). Due to the important role of gapped spin excitations

in the damping of the RM, its energy $E_{\rm r}$ does not critically depend on the superconducting gap energy $2\Delta(T)$ and hence, on temperature and peculiarities of the electronic spectrum in cuprates, contrary to the theories based on the RPA (see, e.g., [9, 15]). In particular, $E_{\rm r}$ is found to be larger than $2\Delta_0$ as observed in experiments (see Figs. 12 and 13).

It should be stressed, that the damping of the RM in our microscopic theory within the t–J model is determined by the kinematic interaction induced by the kinetic energy t of electrons moving in a singly occupied Hubbard subband. This interaction is absent in conventional fermion models in which strong electron correlations are neglected and the spin–electron scattering is determined by a phenomenological interaction with a coupling constant as a fit parameter.

Finally, let us note that our approach, using the MFA for the electronic spectral functions, Eqs. (22) and (23), in the computation of the self-energy (25) has to be considered as a first step towards a fully self-consistent theory of the DSS in the $t-J$ model. However, we believe that the consideration of more accurate fermionic GFs in Eqs. (16) and (17) beyond the Hubbard-I approximation (see, e.g., [29]) should not change our main conclusions, since the shape of the FS and the form of the superconducting gap $2\Delta(\mathbf{q})$ do not play an essential role in our theory, contrary to the spin-exciton scenario.

Partial financial support by the Heisenberg–Landau Program of JINR is acknowledged. One of the authors (N. P.) is grateful to the MPIPKS, Dresden, for the hospitality during his stay at the Institute, where a part of the present work has been done.

APPENDIX A
MODE-COUPLING APPROXIMATION

To calculate the self-energy (4) we use the MCA for the time-dependent multiparticle correlation function which appears in the spectral representation of the relaxation function

$$\begin{aligned} \Sigma''(\mathbf{q},\omega) &= -\frac{1}{2\omega\, m(\mathbf{q})}[I(\mathbf{q},-\omega) - I(\mathbf{q},\omega)], \\ I(\mathbf{q},\omega) &= \int_{-\infty}^{\infty} dt\, e^{i\omega t} \langle\, \ddot{S}^{-}_{\mathbf{q}} | \ddot{S}^{+}_{-\mathbf{q}}(t)\rangle^{\rm proper}, \end{aligned} \tag{27}$$

where

$$-\ddot{S}^{+}_{i} = [[S^{+}_{i},\, (H_t + H_J)], (H_t + H_J)] \equiv \sum_{\alpha} F^{\alpha}_{i} \tag{28}$$

determines the force correlation functions of the force operators F^{α}_{i} denoted by the index $\alpha = tt,\, tJ,\, Jt,\, JJ$. As discussed in [24], at a sizeable doping $\delta \sim 0.1$

considered in this paper, only the term F_i^{tt} can be taken into account, since all other terms give negligible contributions. For this term we have

$$\begin{aligned} F_i^{tt} &= \sum_{j,n} t_{ij} \Big\{ t_{jn} \left[H_{ijn}^{-} + H_{nji}^{+} \right] - t_{in} \left[H_{jin}^{-} + H_{nij}^{+} \right] \Big\}, \\ H_{ijn}^{\sigma} &= X_i^{\sigma 0} X_j^{+-} X_n^{0\sigma} + X_i^{+0} (X_j^{00} + X_j^{\sigma\sigma}) X_n^{0-}. \end{aligned} \tag{29}$$

Following the reasoning of [24], in Eq. (29) only products of operators on different sites are taken into account. After the Fourier transformation to the $\mathbf{q}$-space we obtain the force–force correlation function

$$\begin{aligned} &\langle\, [F_{\mathbf{q}}^{tt}]^{\dagger} \mid F_{\mathbf{q}}^{tt}(t) \rangle = (2t)^4 \sum_{\mathbf{q_1},\mathbf{q_2}} \sum_{\mathbf{q}'_1,\mathbf{q}'_2} \\ &\langle [\Lambda_{\mathbf{q}'_1,\mathbf{q}'_2,\mathbf{q}'_3}\, H^{-}_{\mathbf{q}'_1,\mathbf{q}'_2,\mathbf{q}'_3} + \Lambda_{\mathbf{q}'_3,\mathbf{q}'_2,\mathbf{q}'_1}\, H^{+}_{\mathbf{q}'_1,\mathbf{q}'_2,\mathbf{q}'_3}]^{\dagger} \mid \\ &[\Lambda_{\mathbf{q_1},\mathbf{q_2},\mathbf{q_3}}\, H^{-}_{\mathbf{q_1},\mathbf{q_2},\mathbf{q_3}}(t) + \Lambda_{\mathbf{q_3},\mathbf{q_2},\mathbf{q_1}}\, H^{+}_{\mathbf{q_1},\mathbf{q_2},\mathbf{q_3}}(t)] \rangle, \end{aligned} \tag{30}$$

where $\mathbf{q}_3 = \mathbf{q} - \mathbf{q}_1 - \mathbf{q}_2$ and $\mathbf{q'}_3 = \mathbf{q} - \mathbf{q'}_1 - \mathbf{q'}_2$. Here we introduce the vertex function

$$\Lambda_{\mathbf{q}_1\mathbf{q}_2\mathbf{q}_3} = 4(\gamma_{\mathbf{q}_3+\mathbf{q}_2} - \gamma_{\mathbf{q}_1})\, \gamma_{q_3} + \gamma_{\mathbf{q}_2} - \gamma_{\mathbf{q}_1+\mathbf{q}_3}, \tag{31}$$

where the terms linear in $\gamma_{\mathbf{q}}$ reflect the exclusion of terms in F_i^{tt} with coinciding sites.

In the MCA we assume that the propagation of electronic- and bosonic-type excitations at different lattice sites in Eq. (29) occurs independently which results in the decoupling of the correlation function (30) into the corresponding single-particle time-dependent correlation functions. As it turned out by numerical evaluations (see also [24]), the contribution from the charge excitations given by $(X_j^{00} + X_j^{\sigma\sigma})$ in Eq. (29) can be neglected in comparison with the spin-excitation contribution given by $X_j^{+-} = S_j^{+}$. In this approximation we obtain the spin-diagonal correlation functions for the normal state

$$\begin{aligned} \langle [H^{\sigma}_{\mathbf{q}'_1,\mathbf{q}'_2,\mathbf{q}'_3}]^{\dagger} \mid H^{\sigma}_{\mathbf{q_1},\mathbf{q_2},\mathbf{q_3}}(t) \rangle &= \langle X^{\sigma 0}_{\mathbf{q}'_3} S^{-}_{-\mathbf{q}'_2} X^{0\sigma}_{\mathbf{q}'_1} \mid X^{\sigma 0}_{\mathbf{q_1}}(t) S^{+}_{\mathbf{q_2}}(t) X^{0\sigma}_{\mathbf{q_3}}(t) \rangle = \\ &= \langle X^{0\sigma}_{\mathbf{q_1}} X^{\sigma 0}_{\mathbf{q_1}}(t) \rangle \, \langle S^{-}_{-\mathbf{q_2}} S^{+}_{\mathbf{q_2}}(t) \rangle \, \langle X^{\sigma 0}_{\mathbf{q_3}} X^{0\sigma}_{\mathbf{q_3}}(t) \rangle \times \, \delta_{\mathbf{q}_1,\mathbf{q}'_1}\, \delta_{\mathbf{q}_2,\mathbf{q}'_2} \delta_{\mathbf{q}_3,\mathbf{q}'_3}. \end{aligned} \tag{32}$$

In the superconducting state we additionally take into account pair correlation functions which appear in the spin off-diagonal terms

$$\begin{aligned} &\langle [H^{\bar{\sigma}}_{\mathbf{q}'_1,\mathbf{q}'_2,\mathbf{q}'_3}]^{\dagger} | H^{\sigma}_{\mathbf{q_1},\mathbf{q_2},\mathbf{q_3}}(t) \rangle = \langle X^{\bar{\sigma}0}_{\mathbf{q}'_3} S^{-}_{-\mathbf{q}'_2} X^{0\bar{\sigma}}_{\mathbf{q}'_1} | X^{\sigma 0}_{\mathbf{q_1}}(t) S^{+}_{\mathbf{q_2}}(t) X^{0\sigma}_{\mathbf{q_3}}(t) \rangle = \\ &= -\langle X^{0\bar{\sigma}}_{-\mathbf{q_3}} X^{0\sigma}_{\mathbf{q_3}}(t) \rangle \langle S^{-}_{-\mathbf{q_2}} S^{+}_{\mathbf{q_2}}(t) \rangle \langle X^{\bar{\sigma}0}_{-\mathbf{q_1}} X^{\sigma 0}_{\mathbf{q_1}}(t) \rangle \times \delta_{\mathbf{q}_1,-\mathbf{q}'_3} \delta_{\mathbf{q}_2,\mathbf{q}'_2} \delta_{\mathbf{q}_3,-\mathbf{q}'_1}. \end{aligned} \tag{33}$$

By substituting the MCA correlation functions (32) and (33) in Eq. (27) we obtain the multiparticle correlation function

$$I(\mathbf{q},\omega) = \int_{-\infty}^{\infty} dt\, e^{i\omega t} \frac{1}{N^2} \sum_{\mathbf{q_1},\mathbf{q_2}} \langle S^-_{-\mathbf{q_2}} S^+_{\mathbf{q_2}}(t)\rangle \times$$
$$\times \left[(\Lambda^2_{\mathbf{q_1},\mathbf{q_2},\mathbf{q_3}} + \Lambda^2_{\mathbf{q_3},\mathbf{q_2},\mathbf{q_1}}) \langle X^{0\sigma}_{\mathbf{q_1}} X^{\sigma 0}_{\mathbf{q_1}}(t)\rangle \langle X^{\sigma 0}_{\mathbf{q_3}} X^{0\sigma}_{\mathbf{q_3}}(t)\rangle - \right.$$
$$\left. - \Lambda_{\mathbf{q_1},\mathbf{q_2},\mathbf{q_3}} \Lambda_{\mathbf{q_3},\mathbf{q_2},\mathbf{q_1}} \sum_{\sigma} \langle X^{\bar{\sigma}0}_{-\mathbf{q_1}} X^{\sigma 0}_{\mathbf{q_1}}(t)\rangle \langle X^{0\bar{\sigma}}_{-\mathbf{q_3}} X^{0\sigma}_{\mathbf{q_3}}(t)\rangle \right]. \quad (34)$$

Using the spectral representation for the time-dependent correlation functions (see, e.g., [25])

$$\langle BA(t)\rangle = \int_{-\infty}^{\infty} d\omega\, e^{-i\omega t} f(\omega) [-(1/\pi)] \mathrm{Im} \langle\langle A|B\rangle\rangle_{\omega}, \quad (35)$$

where $f(\omega)$ is the Fermi (Bose) function $n(\omega)$ ($N(\omega)$), after integration over time t we derive Eq. (15).

REFERENCES

1. *Bourges Ph.* The Gap Symmetry and Fluctuations in High Temperature Superconductors / Ed. by Bok J., Deutscher G., Pavuna D., Wolf S. A. Plenum Press, 1998. P. 349–371.
2. *Sidis Y. et al.* // phys. stat. sol. (b). 2004. V. 241. P. 1204.
3. *Eschrig M.* // Adv. Phys. 2006. V. 55. P. 47.
4. *He H. et al.* // Science. 2002. V. 295. P. 1045.
5. *Wilson S. D. et al.* // Nature. 2006. V. 442. P. 59.
6. *Stock C. et al.* // Phys. Rev. B. 2004. V. 69. P. 014502.
7. *Stock C. et al.* // Phys. Rev. B. 2005. V. 71. P. 024522.
8. *Stock C. et al.* // Phys. Rev. B. 2008. V. 77. P. 104513.
9. *Eremin I. et al.* // Phys. Rev. Lett. 2005. V. 94. P. 147001.
10. *Manske D., Eremin I., Bennemann K. H.* The Physics of Conventional and Unconventional Superconductors / Ed. by Bennemann K. H. and Ketterson J. B. Berlin: Springer-Verlag, 2004. V. II. P. 731.
11. *Fauqué B. et al.* // Phys. Rev. B. 2007. V. 76. P. 214512.

12. *Pailhés S. et al.* // Phys. Rev. Lett. 2006. V. 96, P. 257001.

13. *Hubbard J.* // Proc. Roy. Soc. A. 1965. V. 285, P. 542.

14. *Izyumov Yu. A., Letfulov B. M.* // J. Phys.: Condens. Matter. 1990. V. 2. P. 8905; *Izyumov Yu. A., Hedersen J. A.* // Int. J. Mod. Phys. B. 1994. V. 8. P. 1877.

15. *Onufrieva F., Pfeuty P.* // Phys. Rev. B. 2002. V. 65. P. 054515.

16. *Mori H.* // Prog. Theor. Phys. 1965. V. 34. P. 399.

17. *Sega I., Prelovšek P., Bonča J.* // Phys. Rev. B. 2003. V. 68. P. 054524.

18. *Prelovšek P., Sega I., Bonča J.* // Phys. Rev. Lett. 2004. V. 92. P. 027002.

19. *Sega I., Prelovšek P.* // Phys. Rev. B. 2006. V. 73. 092516.

20. *Prelovšek P., Sega I.* // Phys. Rev. B. 2006. V. 74. P. 214501.

21. *Sherman A., Schreiber M.* // Phys. Rev. B. 2003. V. 68. P. 094519.

22. *Sherman A., Schreiber M.* // Fiz. Nizk. Temp. (Low Temp. Phys., Ukraine). 2006. V. 32. P. 499.

23. *Vladimirov A. A., Ihle D., Plakida N. M.* // Theor. Math. Phys. 2005. V. 145. P. 1576.

24. *Vladimirov A. A., Ihle D., Plakida N. M.* // Phys. Rev. B. 2009. V. 80. P. 104425.

25. *Zubarev D. N.* // Sov. Phys. Uspekhi. 1960. V. 3. P. 320.

26. *Tserkovnikov Yu. A.* // Theor. Math. Phys. 1981. V. 49. P. 993; Theor. Math. Phys. 1982. V. 52. P. 712.

27. *Won H., Maki K.* // Phys. Rev. B. 1994. V. 49. P. 1397.

28. *Tallon J. L. et al.* // Phys. Rev. B. 1995. V. 51. P. 12911.

29. *Plakida N. M., Oudovenko V. S.* // JETP. 2007. V. 104. P. 230.

Received on May 27, 2010.

Корректор *Т. Е. Попеко*

Подписано в печать 5.07.2010.
Формат 60 × 90/16. Бумага офсетная. Печать офсетная.
Усл. печ. л. 1,68. Уч.-изд. л. 2,24. Тираж 305 экз. Заказ № 57032.

Издательский отдел Объединенного института ядерных исследований
141980, г. Дубна, Московская обл., ул. Жолио-Кюри, 6.
E-mail: publish@jinr.ru
www.jinr.ru/publish/